

Observation of the superconducting proximity effect in the surface state of SmB_6 thin films

Seunghun Lee^{1,2}, Xiaohang Zhang^{1,2}, Yangang Liang², Sean Fackler², Jie Yong^{1,3},
Xiangfeng Wang^{1,3}, Johnpierre Paglione^{1,3}, Richard L. Greene^{1,3}, and Ichiro
Takeuchi^{1,2,*}

¹Center for Nanophysics and Advanced Materials, University of Maryland, College Park,
Maryland 20742, USA

²Department of Materials Science and Engineering, University of Maryland, College Park,
Maryland 20742, USA

³Department of Physics, University of Maryland, College Park, Maryland 20742, USA

*Corresponding author (email: takeuchi@umd.edu)

(Dated on April 5, 2016)

ABSTRACT

The proximity effect at the interface between a topological insulator (TI) and a superconductor is predicted to give rise to chiral topological superconductivity and Majorana fermion excitations. In most TIs studied to date, however, the conducting bulk states have overwhelmed the transport properties and precluded the investigation of the interplay of the topological surface state and Cooper pairs. Here, we demonstrate the superconducting proximity effect in the surface state of SmB_6 thin films which display bulk insulation at low temperatures. The Fermi velocity in the surface state deduced from the proximity effect is found to be as large as 10^5 m/s, in good agreement with the value obtained from a separate transport measurement. We show that high transparency between the TI and a superconductor

is crucial for the proximity effect. The finding here opens the door to investigation of exotic quantum phenomena using all-thin-film multilayers with high-transparency interfaces.

I. INTRODUCTION

Topological insulators (TI), which show exotic metallic surfaces with insulating bulk, have attracted tremendous interest in the condensed matter physics community. The topologically protected surface state of TI has been regarded as a promising platform for exploring exotic quantum phenomena in solid materials. In particular, it has been suggested that the superconducting proximity effect occurring at an interface between a TI and a superconductor may give rise to chiral topological superconductivity[1-3] and Majorana fermion excitations[4-9]. To this end, concerted experimental efforts have been made to study the superconducting proximity effect in superconductor/TI bilayer structures. However, in most Bi- and Te-based TI such as Bi_2Se_3 , Bi_2Te_3 , Sb_2Te_3 , etc., the overwhelming conducting bulk electronic states hinder interfacial quantum phenomena and preclude the investigation of the interplay of the topological surface state and Cooper pairs[10-13]. In addition, low transparency at the superconductor/TI interface due to a non-pristine surface of the TI can significantly reduce the extent of the proximity effect[5,14-16]. Therefore, suppressing the bulk conductivity and securing high interfacial transparency in superconductor/TI bilayers have been an outstanding issue in this field.

Samarium hexaboride (SmB_6) has recently emerged as an ideal material to explore TI-based quantum phenomena because of its true insulating bulk[17]. To date, many theoretical and experimental studies have provided strong evidence for the existence of the conducting surface state and a robust insulating bulk of SmB_6 at low temperatures[18-37]. Specifically, electronic transport measurements on SmB_6 single crystals have revealed surface current

dominated conduction[20,31] and thickness-independent Hall voltage at low temperatures due to the conducting surface[20]. A point contact spectroscopy (PCS) study has indicated the presence of an insulating bulk in SmB₆ at low temperatures[23,38]. The electronic structures of SmB₆ obtained by ARPES and a quantum oscillation measurement with torque magnetometry are consistent with theoretical predictions, *e.g.*, presence of an odd number of Dirac surface bands[19,34,39]. However, there still remain many questions regarding the nature of the surface state of SmB₆ including the origin of the metallic surface state and whether the surface state is truly topologically protected[17,22,27,40-42].

In this paper, we demonstrate direct observation of the proximity effect induced in the surface state of SmB₆ for the first time. We apply the Usadel formalism to the systematic change in the superconducting transition temperature of a series of *in-situ* deposited SmB₆/Nb bilayers with different Nb layer thicknesses and arrive at the normal coherence length of the surface state of SmB₆ to be ≈ 10 nm. From a separate transport study on SmB₆ thin films, we find the thickness of the surface state to be ≈ 7 nm. The Fermi velocity (v_F) obtained from the transport measurements is in good agreement with v_F calculated using the normal coherence length, and it is of the order of 10^5 m/s. These numbers paint a picture of a material whose bulk insulation provides a unique opportunity to probing and exploiting its surface state in thin-film multilayer devices.

II. METHODS

SmB₆ thin films were prepared by co-sputtering of SmB₆ and B targets; additional B sputtering was performed for compensating B deficiency and the base pressure was $\sim 2 \times 10^{-8}$ Torr. The thin films were grown on Si (100) substrate at 800°C in an atmosphere of Ar

(99.999%) and the working pressure was kept at 10 mTorr. After deposition, further annealing process was performed at 800°C for 3 hours in high vacuum. X-ray diffraction and transmission electron microscopy results can be found in the reference[37]. For fabricating Nb/SmB₆ bilayers, Nb layer were prepared on SmB₆ by sputtering method both *in-situ* and *ex-situ* at room temperature. The base pressure was $\sim 2 \times 10^{-8}$ Torr and the working pressure was kept at 7 mTorr. For fabricating Nb/Au bilayer, Au layer was prepared on Si substrate by thermal evaporator and the base pressure was $\sim 10^{-6}$ Torr.

The electrical properties were measured by Physical properties measurement system (PPMS). Temperature-dependent resistance for T_c evaluation was measured by simple 4-point probe method with 0.01 K step. Electrical contacts were made with an Al wire-bonder, and the typical contact resistance was $\sim 1 \Omega$. Transport characteristics of SmB₆ thin films were measured with Hall bar geometry; six-contact 1-2-2-1 Hall bars with 200 μm channel size were prepared by ion milling process.

III. RESULTS AND DISCUSSION

A. Transport characteristics

We performed transport measurements on SmB₆ thin films with varying film thickness. In order to perform the transport measurements, each film was patterned into a Hall-bar with a channel width of 200 μm . Resistance vs. temperature (R-T) was measured for all SmB₆ films, and their sheet conductance (G_{\square}) values at 300 K and 2 K are plotted in Figure 1. The G_{\square} was calculated using $G_{\square} = G \cdot a/w$, where a and w are the length and the width of the Hall bar channels, respectively. All samples show a nearly constant resistance value at low temperatures. The inset shows a representative R-T curve for a 25 nm thin film. The result is consistent with previous reports[24,29,31,35] where a saturation of resistance (*i.e.*, plateau)

has been attributed to the transition from bulk state-dominated conduction to surface state-dominated conduction at low temperatures.

To see if there is any thickness dependent effect in our samples, we plot G_{\square} at 2 K and 300 K as a function of film thickness (Figure 1). G_{\square} at 300 K clearly displays a linear thickness dependence, indicating bulk transport. However, if the resistance plateau at low temperatures arises from the surface conduction, G_{\square} at 2 K should be independent of the thickness and become a constant. This is indeed the case, as seen in Fig. 1, strongly suggestive of the presence of the surface conduction channel. We also measured the Hall resistance (R_{xy}) as a function of magnetic field, and calculated the sheet carrier concentration and the mobility of the SmB₆ thin films at 2 K. Both were found to be constant and independent of the film thickness (Supplementary Info.).

To determine the thickness of the surface conduction channel, we adopt a simple parallel conductance model where the electronic conduction is through two channels: a surface channel including contributions from both the top and the bottom surfaces and a bulk channel[24,31,43]. This model is valid for the temperature region where the Kondo gap of SmB₆ opens, which is a sufficient condition for the emergence of the topological surface state. Therefore, we apply this model to the transport results in a temperature range below 120 K, at which the Kondo gap starts to open in SmB₆[23]. The conductance of the surface channel is assumed to be temperature independent, and that of the bulk channel is temperature dependent and it can be described by a bulk resistivity and exponential function (*i.e.*, Arrhenius equation). The total conductance of the SmB₆ thin film can then be described as:

$$G = G_{surface} + G_{bulk} \quad (1)$$

$$G_{surface} = \frac{w}{a} G_{\square,2K}, \quad G_{bulk} = \frac{w \cdot t_{bulk}}{a} \cdot \sigma_{bulk,300K} \exp\left(-\frac{E_a}{k_B T} + \frac{E_a}{300k_B}\right) \quad (2)$$

The use of the bulk conductivity in the G_{bulk} term allows us to add a thickness of bulk channel (t_{bulk}) as fitting parameters, and subsequently to estimate a thickness of surface channel ($t_{surface}$) because the total film thickness is $2t_{surface} + t_{bulk}$. The bulk conductivity, $\sigma_{bulk,300K}$, is $7.66 \times 10^5 \text{ S m}^{-1}$ which is the slope of G_{\square} at 300 K obtained from the data shown in Fig. 1. $G_{\square,2K}$ is the G_{\square} at 2 K for each sample, and a and w are the length and the width of the Hall bar channel, respectively. Fitting parameters are t_{bulk} and E_a , where E_a is an activation energy. We fit the data for all samples using the equation (1) and (2). A representative fitting result is shown in Fig. 2a. The values of fitting parameters E_a and $t_{surface}$ for the different thickness samples are shown in Figure 2b, and $t_{surface}$ is the thickness of the surface conduction channel, *i.e.*, the thickness of the surface state of SmB_6 . Both E_a and $t_{surface}$ are found to be constant regardless of the film thickness. The average value of E_a is $2.73 \pm 0.04 \text{ meV}$, which is in good agreement with the values obtained from SmB_6 single crystals[24,28,44].

From the above analysis, we obtain $t_{surface} \approx 7 \text{ nm}$. To obtain v_F , we used $v_F = E_g t_{surface} / \hbar$ derived from the solution of the effective low-energy Hamiltonian for topological insulators with a surface state where E_g is the bulk energy gap[29,45]. We use E_g of 17 meV measured on our SmB_6 thin films by terahertz spectroscopy[46], which is also in agreement with the values obtained from single crystal SmB_6 using point contact spectroscopy[23], scanning tunneling spectroscopy[25], etc. With $E_g = 17 \text{ meV}$ and $t_{surface} = 7 \text{ nm}$, we arrive at $v_F \sim 1.8 \times 10^5 \text{ m/s}$, a value close to that measured in quantum oscillation measurements on single crystal SmB_6 [19]. This value is also in agreement with an independent estimate of v_F obtained from the proximity effect study as discussed below.

B. Proximity effect

The superconducting proximity effect describes a phenomenon at a superconductor-normal metal interface where Cooper pairs diffuse into the normal metal resulting in the suppression of the critical temperature (T_c) of the superconductor while inducing surface or local superconductivity in the normal metal. We fabricated Nb/SmB₆ bilayers and observed a change in T_c depending on the thickness of Nb layer due to the proximity effect at the interface. To characterize the proximity effect of the bilayers, we treat the Nb/SmB₆ bilayer as a superconductor/metal bilayer system, where the metallic layer in SmB₆ is the surface conducting channel (Figure 3), and we calculate the normal coherence length (ξ) and v_F of SmB₆ thin films using the Usadel equation[16,47,48]. Assuming that ξ of SmB₆ (ξ_{SmB_6}) is longer than the thickness of the surface conducting channel of SmB₆ ($\xi_{\text{SmB}_6} > t_{\text{surface}}$), the fitting equation for evaluating ξ_{SmB_6} can be obtained by linearizing the Usadel equation[16]:

$$\frac{T_{cb}}{T_{cs}} = 1 - \frac{\pi^2}{4} \frac{\xi_{\text{Nb}}}{d_{\text{Nb}}} \gamma \cdot p(\gamma) \quad (3)$$

$$\gamma = \frac{\rho_{\text{Nb}} \xi_{\text{Nb}} t_{\text{surface}}}{\rho_{\text{SmB}_6} (\xi_{\text{SmB}_6})^2} \quad (4)$$

$$p(\gamma) = 1.17 + \frac{2}{\pi^2} \ln(1 + 0.98\gamma^{-2}) \quad (5)$$

where T_{cb} and T_{cs} represent the T_c of the Nb/SmB₆ bilayer and the T_c of a single Nb layer, respectively. T_{cb} is evaluated by the Ginzburg-Landau equation, and γ and $p(\gamma)$ are approximated by the expressions above[16]. γ represents the strength of the proximity effect between layers[47]. ρ_{Nb} and ρ_{SmB_6} are the residual resistivities of the Nb layer and the SmB₆ layer, respectively. ξ_{Nb} and ξ_{SmB_6} are the coherence length of the Nb layer and the SmB₆ layer, respectively. d_{Nb} is the thickness of the Nb layer. To check the validity of the model, a series

of Nb/Au bilayers were also fabricated, and the extracted value of ζ_{Au} was in good agreement with their known value ($\sim 1\mu\text{m}$).

For Nb/SmB₆ bilayers, d_{Nb} was varied from 20 to 100 nm, and the thickness of SmB₆ layer was fixed to be 50 nm. Figure 4a and 4b show the resistance vs. temperature curves of single Nb layers and Nb/SmB₆ bilayers near T_c for different thicknesses of the Nb layer (d_{Nb}) respectively. Each resistance curve was normalized by a value obtained at a temperature slightly above the transition temperature. The T_c of single Nb layer gradually decreases with decreased d_{Nb} due to localization[49] and each Nb/SmB₆ bilayer has a lower T_c than the corresponding Nb single layer due to the proximity effect established between Nb and SmB₆ layers. Based on x-ray diffraction and cross-sectional SEM of the bilayers, we do not believe there is any significant diffusion at the interface.

Figure 4c shows the T_{cb}/T_{cs} of the Nb/SmB₆ system as a function of d_{Nb} . As a comparison, one bilayer was made with an *ex-situ* interface: following the deposition of SmB₆, it was exposed to air before the Nb layer was deposited. As represented in Fig. 4c, this sample shows a much higher T_{cb}/T_{cs} (*i.e.*, higher T_c) than the corresponding *in-situ* bilayer. The proximity effect is very sensitive to the nature of the top most layer of SmB₆. Specifically, degradation of the top most surface layer (*e.g.*, due to oxidation) may reduce the boundary transparency, resulting in reduction of the proximity effect. This result demonstrates that *in-situ* formed multilayers with clean interfaces are critical for establishing such a proximity effect at the interface of SmB₆.

To evaluate ζ_{SmB_6} , we performed a fitting process based on the expression discussed above. Using measured values of $\rho_{\text{Nb}} = 8.5 \times 10^{-6} \Omega \cdot \text{cm}$, the mean free path (l) of Nb was estimated

from $\rho_{\text{Nb}}l = 3.75 \times 10^{-6} \mu\Omega \cdot \text{cm}^2$ [50] (*i.e.*, $l = 4.4$ nm) and we obtain $\zeta_{\text{Nb}} = 0.852(\zeta_{\text{Nb(bulk)}}l)^{1/2} = 11$ nm where $\zeta_{\text{Nb(bulk)}}$ is the known value of coherence length of Nb bulk ($\zeta_{\text{Nb(bulk)}} = 38$ nm)[51]. The thickness of the surface conducting channel of SmB₆ has been evaluated from our transport result ($t_{\text{surface}} = 7$ nm), and the resistivity of the surface state was calculated to be $8.96 \times 10^{-5} \Omega \cdot \text{cm}$ ($= \rho_{\text{SmB}_6}$) at 2 K based on the above measured sheet conductance ($\rho = 2t_{\text{surface}}/G_{\square}$). The only unknown parameter is ζ_{SmB_6} . The fitting result is shown as a red solid line in Fig. 4c, and we arrive at ζ_{SmB_6} of 9.6 nm. To calculate v_F , $\zeta = (v_F \hbar l / 6\pi k_B T)^{1/2}$ is used[52], where l of the SmB₆ thin film was assumed to be the grain size of our SmB₆ film, ≈ 4 nm[37], and we obtain $v_F \approx 10^5$ m/s at 2 K for SmB₆. This v_F is comparable to the value obtained from the transport study above ($v_F = 1.8 \times 10^5$ m/s), which implies that the observed superconducting proximity effect is attributed to the surface state of SmB₆ thin film. As a comparison, we have also carried out a fit using entire bulk of the SmB₆ thin film (even though, we have shown above that the bulk of the film is insulating): in this case, the fit does not provide a v_F value consistent with the v_F value obtained from the transport study. Our bilayer fabrication method in ultra high vacuum process excludes any degradation or contamination as the origin of the metallic surface state.

The value of v_F and the effective mass of quasiparticles in the surface state of SmB₆ have been the subjects of much debate. Early theoretical calculations had suggested the presence of relatively heavy Dirac quasiparticles with small v_F ($\sim 10^3$ m/s)[26,53] in the topologically protected surface state, while recent APRES and quantum oscillation studies have pointed to light quasiparticles with large v_F of $> 10^4$ m/s[19][32,33]. To resolve the discrepancy, Alexandrov *et al.* have recently proposed that Kondo breakdown at the surface of SmB₆ could release unquenched moments at the surface, causing the Dirac point to shift down into the valence band and giving rise to large v_F values[54]. We have examined the Sm valence

state in the surface of our SmB₆ thin films using x-ray photoemission spectroscopy at room temperature and found that it is similar to that of SmB₆ single crystals, which is ~ 2.7 [55] (Supplementary Info.). Therefore, we exclude chemical extrinsic effects as the origin of the large v_F value observed here. We believe our high v_F value is also due to the Kondo breakdown effect[54]. We note that $t_{surface}$ of ≈ 7 nm found in this study is consistent with the thickness predicted with the Kondo breakdown effect[54]. It has been reported that SmB₆ has three Dirac cones, each with its own slightly different value of v_F [32,39] The measured v_F in this study is therefore expected to be the average v_F of the three Dirac cones.

With the ζ_{SmB_6} obtained from the fitting above, we are able to evaluate γ which is a measure of the strength of the superconducting proximity effect. The values of γ for *in-situ* and *ex-situ* bilayer are 7.9×10^{-2} and 1.0×10^{-2} , respectively. This implies that the strength of the proximity effect of the *in-situ* sample is roughly 8 times larger than that of the *ex-situ* sample. The strength of the superconducting proximity effect is naturally one of the most important factors in superconductor – normal– superconductor Josephson junctions, and it directly affects the $I_C R_N$ product. It is interesting to note that significantly reduced $I_C R_N$ products, presumably due to lack of the pristine surface of the TI during the fabrication process, have been observed in various studies on chalcogenide-TI-based Josephson junctions[5,6]. Specifically, the observed $I_C R_N$ products in such studies are typically around 20 μ V, which is far below the theoretical value, *i.e.*, $I_C R_N \sim \pi \Delta(0)/2e \approx 4.7$ mV, for junctions in the clean limit [56][57]. Higher $I_C R_N$ product junctions (and in particular high I_C junctions) are always desirable for investigating novel quantum phenomena involving coherence of superconductivity, where signature of such phenomena might appear in the form of small modulation in the critical current. The present study shows that the strength of proximity effect in the bilayer with an *in-situ* interface is nearly an order of magnitude higher than that

with an *ex-situ* interface. We expect that with identical geometric dimensions, junctions fabricated by *in-situ* interface may display a substantially larger $I_C R_N$ than junctions fabricated with *ex-situ* interface. Thus, we have demonstrated an important pre-requisite for attaining a high $I_C R_N$ junction. A non-ideal S/N interface such as one with a thin tunnel barrier (formed due to an *ex-situ* process) can result in scattering at the interface leading to decoherence[7,58]. This may be the reason why the proposed signatures of Majorana fermions have not been observed in Josephson junctions to date.

IV. CONCLUSIONS

In summary, thickness-independent behavior in the transport properties was observed in ultrathin SmB₆ films, and the thickness of the surface state was deduced to be ≈ 7 nm. We provide first direct evidence of the superconducting proximity effect in the surface state of SmB₆ through pristine interfaces with *in-situ* deposited Nb layers. The Fermi velocity values of the surface state obtained from the transport measurements and the proximity effect are in good agreement with each other. The present work lays the groundwork for fabricating SmB₆ thin film based multilayers and devices for investigating quantum phenomena including Majorana fermion excitations.

ACKNOWLEDGEMENT

The authors would like to acknowledge professor Victor Galitski for valuable discussions. This work was supported by AFOSR (FA95501410332) and NSF grants (DMR-1410665 and DMR-1410665). It was also supported by the Maryland NanoCenter.

REFERENCES

- [1] A. C. Potter and P. A. Lee, *Engineering a $p+ip$ superconductor: Comparison of topological insulator and Rashba spin-orbit-coupled materials*, Phys. Rev. B **83**, 184520 (2011).
- [2] X.-L. Qi, T. L. Hughes, and S.-C. Zhang, *Chiral topological superconductor from the quantum Hall state*, Phys. Rev. B **82**, 184516 (2010).
- [3] X.-L. Qi, T. L. Hughes, and S.-C. Zhang, *Topological field theory of time-reversal invariant insulators*, Phys. Rev. B **78**, 195424 (2008).
- [4] J. Moore, *Extraordinary Josephson Junction*, Physics **5**, 84 (2012).
- [5] M. Veldhorst *et al.*, *Josephson supercurrent through a topological insulator surface state*, Nat. Mater. **11**, 417 (2012).
- [6] J. R. Williams, A. J. Bestwick, P. Gallagher, S. S. Hong, Y. Cui, A. S. Bleich, J. G. Analytis, I. R. Fisher, and D. Goldhaber-Gordon, *Unconventional Josephson effect in hybrid superconductor-topological insulator devices*, Phys. Rev. Lett. **109**, 056803 (2012).
- [7] L. Fu and C. L. Kane, *Superconducting proximity effect and Majorana fermions at the surface of a topological insulator*, Phys. Rev. Lett. **100**, 096407 (2008).
- [8] F. Yang *et al.*, *Proximity-effect-induced superconducting phase in the topological insulator*, Phys. Rev. B **86**, 134504 (2012).
- [9] C. Nayak, S. H. Simon, A. Stern, M. Freedman, and S. Das Sarma, *Non-Abelian anyons and topological quantum computation*, Rev. Mod. Phys. **80**, 1083 (2008).
- [10] L. Galletti *et al.*, *Influence of topological edge states on the properties of Al/Bi₂Se₃/Al hybrid Josephson devices*, Phys. Rev. B **89**, 134512 (2014).
- [11] B. Sacépé, J. B. Oostinga, J. Li, A. Ubaldini, N. J. G. Couto, E. Giannini, and A. F. Morpurgo, *Gate-tuned normal and superconducting transport at the surface of a*

- topological insulator*, Nat. Commun. **2**:575 (2011).
- [12] M. Snelder *et al.*, *Josephson supercurrent in a topological insulator without a bulk shunt*. Supercond. Sci. Technol. **27**, 104001 (2014).
- [13] G. Koren and T. Kirzhner, *Zero-energy bound states in tunneling conductance spectra at the interface of an s-wave superconductor and a topological insulator in NbN/Bi₂Se₃/Au thin-film junctions*, Phys. Rev. B **86**, 144508 (2012).
- [14] Y. Tanaka, T. Yokoyama, and N. Nagaosa, *Manipulation of the Majorana fermion, Andreev reflection, and Josephson current on topological insulators*, Phys. Rev. Lett. **103**, 107002 (2009).
- [15] G. Koren, *Proximity effects at the interface of a superconductor and a topological insulator in NbN-Bi₂Se₃ thin film bilayers*, Supercond. Sci. Technol. **28**, 1 (2014).
- [16] A. A. Golubov, M. Y. Kupriyanov, V. F. Lukichev, and A. A. Orlikovskii, *Critical-Temperature of a SN Sandwich*, Soviet Microelectronics **12**, 191 (1983).
- [17] M. Dzero, J. Xia, V. Galitski, and P. Coleman, *Topological Kondo Insulators*, arXiv:1506.05635.
- [18] J. W. Allen, B. Batlogg, and P. Wachter, *Large low-temperature Hall effect and resistivity in mixed-valent SmB₆*, Phys. Rev. B **20**, 4807 (1979).
- [19] G. Li *et al.*, *Two-dimensional Fermi surfaces in Kondo insulator SmB₆*, Science **346**, 1208 (2014).
- [20] D. J. Kim, S. Thomas, T. Grant, J. Botimer, Z. Fisk, and J. Xia, *Surface Hall effect and nonlocal transport in SmB₆: Evidence for surface conduction*, Sci. Rep. **3**:3150 (2013).
- [21] S. Rößler, T.-H. Jang, D.-J. Kim, L. H. Tjeng, Z. Fisk, F. Steglich, and S. Wirth, *Hybridization gap and Fano resonance in SmB₆*, Proc. Natl. Acad. Sci. U.S.A. **111**, 4798 (2014).

- [22] W. A. Phelan, S. M. Koochpayeh, P. Cottingham, J. W. Freeland, J. C. Leiner, C. L. Broholm, and T. M. McQueen, *Correlation between bulk thermodynamic measurements and the low-temperature-resistance plateau in SmB_6* , Phys. Rev. X **4**, 031012 (2014).
- [23] X. Zhang, N. P. Butch, P. Syers, S. Ziemak, R. L. Greene, and J. Paglione, *Hybridization, inter-ion correlation, and surface states in the Kondo insulator SmB_6* , Phys. Rev. X **3**, 011011 (2013).
- [24] P. Syers, D. Kim, M. S. Fuhrer, and J. Paglione, *Tuning bulk and surface conduction in the proposed topological Kondo insulator SmB_6* , Phys. Rev. Lett. **114**, 096601 (2015).
- [25] W. Ruan, C. Ye, M. Guo, F. Chen, X. Chen, G.-M. Zhang, and Y. Wang, *Emergence of a coherent in-gap state in the SmB_6 Kondo insulator revealed by scanning tunneling spectroscopy*, Phys. Rev. Lett. **112**, 136401 (2014).
- [26] V. Alexandrov, M. Dzero, and P. Coleman, *Cubic topological Kondo insulators*, Phys. Rev. Lett. **111**, 226403 (2013).
- [27] Z. H. Zhu *et al.*, *Polarity-driven surface metallicity in SmB_6* , Phys. Rev. Lett. **111**, 216402 (2013).
- [28] C. Cooley, M. C. Aronson, Z. Fisk, and P. C. Canfield, *SmB_6 - Kondo insulator or exotic metal*, Phys. Rev. Lett. **74**, 1629 (1995).
- [29] N. Wakeham, Y. Q. Wang, Z. Fisk, F. Ronning, and J. D. Thompson, *Surface state reconstruction in ion-damaged SmB_6* , Phys. Rev. B **91**, 085107 (2015).
- [30] B. Roy, J. D. Sau, M. Dzero, and V. Galitski, *Surface theory of a family of topological Kondo insulators*, Phys. Rev. B **90**, 155314 (2014).
- [31] S. Wolgast, Ç. Kurdak, K. Sun, J. W. Allen, D.-J. Kim, and Z. Fisk, *Low-temperature surface conduction in the Kondo insulator SmB_6* , Phys. Rev. B **88**,

- 180405 (2013).
- [32] J. Jiang *et al.*, *Observation of possible topological in-gap surface states in the Kondo insulator SmB_6 by photoemission*, Nat. Commun. **4**:3010 (2013).
- [33] M. Neupane *et al.*, *Surface electronic structure of the topological Kondo-insulator candidate correlated electron system SmB_6* , Nat. Commun. **4**:2991 (2013).
- [34] N. Xu *et al.*, *Direct observation of the spin texture in SmB_6 as evidence of the topological Kondo insulator*, Nat. Commun. **5**:4566 (2014).
- [35] D. J. Kim, J. Xia, and Z. Fisk, *Topological surface state in the Kondo insulator samarium hexaboride*, Nat. Mater. **13**, 466 (2014).
- [36] J. Yong, Y. Jiang, X. Zhang, J. Shin, I. Takeuchi, and R. L. Greene, *Magnetotransport in nanocrystalline SmB_6 thin films*, AIP Adv. **5**, 077144 (2015).
- [37] J. Yong, Y. Jiang, D. Usanmaz, S. Curtarolo, X. Zhang, L. Li, X. Pan, J. Shin, I. Takeuchi, and R. L. Greene, *Robust topological surface state in Kondo insulator SmB_6 thin films*, Appl. Phys. Lett. **105**, 222403 (2014).
- [38] M. M. Yee, Y. He, A. Soumyanarayanan, D.-J. Kim, Z. Fisk, and J. E. Hoffman, *Imaging the Kondo insulating gap on SmB_6* , arXiv:1308.1085v2.
- [39] F. Lu, J. Zhao, H. Weng, Z. Fang, and X. Dai, *Correlated topological Insulators with mixed valence*, Phys. Rev. Lett. **110**, 096401 (2013).
- [40] P. Hlawenka *et al.*, *Samarium hexaboride: A trivial surface conductor*, arXiv:1502.01542.
- [41] B. S. Tan *et al.*, *Unconventional Fermi surface in an insulating state*, Science **349**, 287 (2015).
- [42] J. D. Denlinger *et al.*, *Consistency of Photoemission and Quantum Oscillations for Surface States of SmB_6* , arXiv:1601.07408v1.
- [43] B. Xia, P. Ren, A. Sulaev, P. Liu, S.-Q. Shen, and L. Wang, *Indications of surface-*

- dominated transport in single crystalline nanoflake devices of topological insulator $Bi_{1.5}Sb_{0.5}Te_{1.8}Se_{1.2}$* , Phys. Rev. B **87**, 085442 (2013).
- [44] S. Wolgast *et al.*, *Magnetotransport measurements of the surface states of samarium hexaboride using Corbino structures*, Phys. Rev. B **92**, 115110 (2015)..
- [45] J. Linder, T. Yokoyama, and A. Sudbø, *Anomalous finite size effects on surface states in the topological insulator Bi_2Se_3* , Phys. Rev. B **80**, 205401 (2009).
- [46] J. Zhang, J. Yong, I. Takeuchi, R. L. Greene, and R. D. Averitt, *Ultrafast terahertz spectroscopy study of Kondo insulating thin film SmB_6 : evidence for an emergent surface state*, arXiv:1509.04688.
- [47] A. A. Golubov, *Proximity effect in dirty N/S multilayers*, OE/LASE '94 **2157**, 353 (1994).
- [48] K. D. Usadel, *Generalized diffusion equation for superconducting alloys*, Phys. Rev. Lett. **25**, 507 (1970)..
- [49] M. S. M. Minhaj, S. Meepagala, J. T. Chen, and L. E. Wenger, *Thickness dependence on the superconducting properties of thin Nb films*, Phys. Rev. B **49**, 15235 (1994).
- [50] A. F. Mayadas, R. B. Laibowitz, and J. J. Cuomo, *Electrical characteristics of rf-sputtered single-crystal niobium films*, J. Appl. Phys. **43**, 1287 (1972).
- [51] C. Delacour, L. Ortega, M. Faucher, T. Crozes, T. Fournier, B. Pannetier, and V. Bouchiat, *Persistence of superconductivity in niobium ultrathin films grown on R-plane sapphire*, Phys. Rev. B **83**, 144504 (2011).
- [52] P. Seidel, *Applied Superconductivity: Handbook on Devices and Applications* (John Wiley & Sons, 2015)
- [53] M. Dzero, K. Sun, P. Coleman, and V. Galitski, *Theory of topological Kondo insulators*, Phys. Rev. B **85**, 045130 (2012)

- [54] V. Alexandrov, P. Coleman, and O. Erten, *Kondo breakdown in topological Kondo insulators*, Phys. Rev. Lett. **114**, 177202 (2015).
- [55] J. N. Chazalviel, M. Campagna, and G. K. Wertheim, *Study of valence mixing in SmB_6 by x-ray photoelectron spectroscopy*, Phys. Rev. B **14**, 4586 (1976).
- [56] M. Tinkham, *Introduction to Superconductivity* (McGraw-Hill, 1996).
- [57] C. Kittel, *Introduction to Solid State Physics* (Wiley, 2005).
- [58] A. Tesauro, A. Aurigemma, C. Cirillo, S. L. Prischepa, M. Salvato, and C. Attanasio, *Interface transparency and proximity effect in Nb/Cu triple layers realized by sputtering and molecular beam epitaxy*, Supercond. Sci. Technol. **18**, 1 (2004)..

Figures and captions

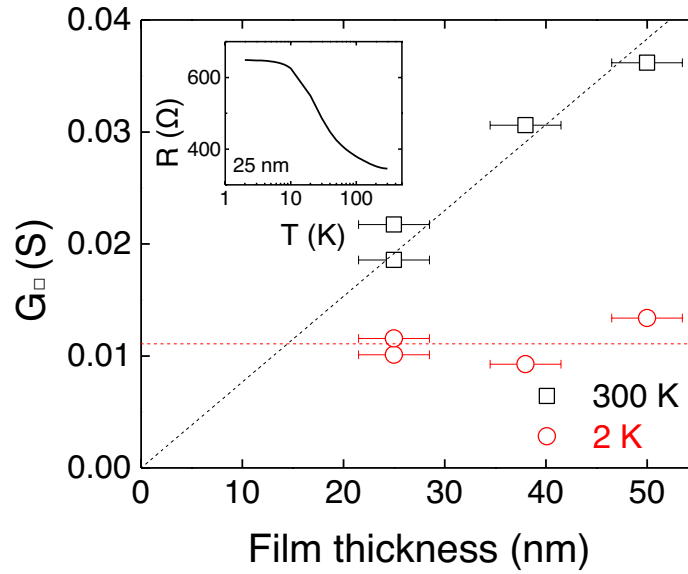


Figure 1. Sheet conductance (G_{\square}) of SmB_6 thin films at 2 K and 300 K as a function of thin thickness Dashed lines are linear fits to the experimental results. The slope of 300 K data represents 3D bulk conductivity at 300 K in SmB_6 thin films, and the fit to the data (black dot line) extrapolates to zero at zero thickness, consistent with the fact that the conduction in SmB_6 thin films is dominated by a 3D bulk transport at 300 K. At 2 K, G_{\square} is independent to the thickness, and the guide line (red dot line) is the fit to the data, which indicates the average value of G_{\square} at 2 K. The inset shows resistance vs. temperature curve for a 25 nm SmB_6 thin film.

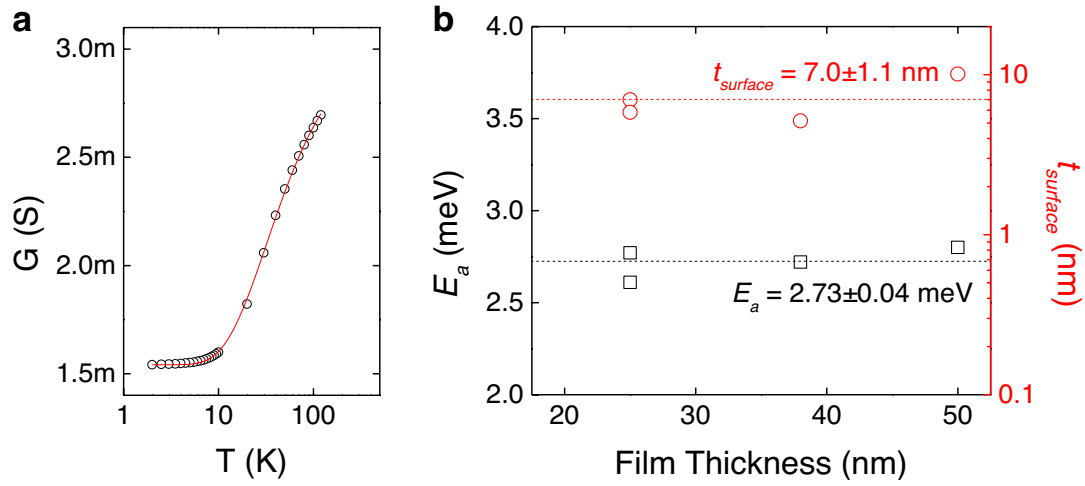


Figure 2. Estimating the thickness of the surface conduction channel in SmB_6 thin films (a) Conductance vs. temperature of a 25 nm SmB_6 thin film. The red line is a best fit to the experimental data using the parallel conductance model. **(b)** Activation energy (E_a) and the thickness of the surface conduction channel (t_{surface}) extracted from the fit as a function of the film thickness for SmB_6 .

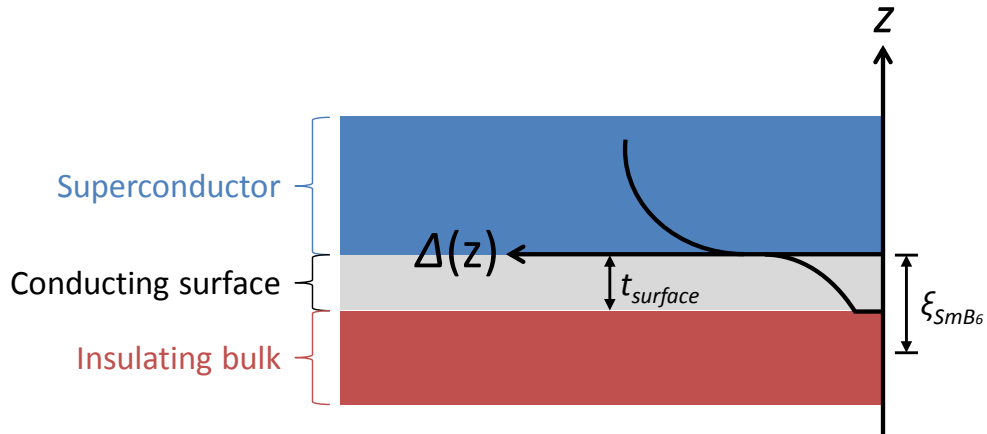


Figure 3. Model for the proximity effect for superconducting/TI system Given the surface conducting channel of the SmB_6 as discussed above, we adopt the model of the proximity effect for the superconducting layer and the surface conduction channel, the surface state of SmB_6 . The plot in the schematic represents the evolution of the superconducting pair potential ($\Delta(z)$). In this model, we consider the case where ξ of SmB_6 (ξ_{SmB_6}) is larger than the thickness of the surface state of SmB_6 (t_{surface}).

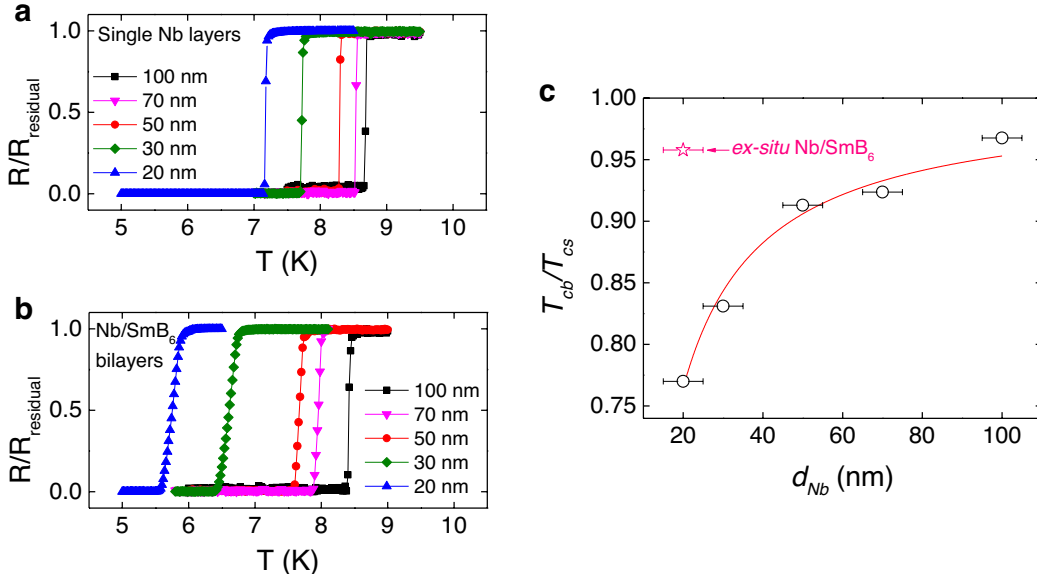


Figure 4. Proximity effect in Nb/SmB₆ bilayer. Resistance vs. temperature curves of (a) single Nb layers and (b) Nb/SmB₆ bilayers for different thickness of Nb layers (d_{Nb}) where the thickness of the SmB₆ layer is fixed to be 50 nm. Each Nb layer was deposited on SmB₆ *in-situ*. The resistance values are normalized by a value obtained at a temperature slightly above the transition temperature (R_{residual}). (c) T_{cb}/T_{cs} (*i.e.*, ratio of T_c of Nb/SmB₆ bilayer to T_c of single Nb layer) as a function of d_{Nb} . The solid line is a fit using the Usadel equation. The star symbol in Fig. 4c indicates T_{cb}/T_{cs} of the Nb/SmB₆ bilayer where 20 nm Nb was deposited on SmB₆ after its surface was first exposed to air forming an *ex-situ* interface with low transparency.

Supplementary Information

- Thickness independent carrier concentration and mobility

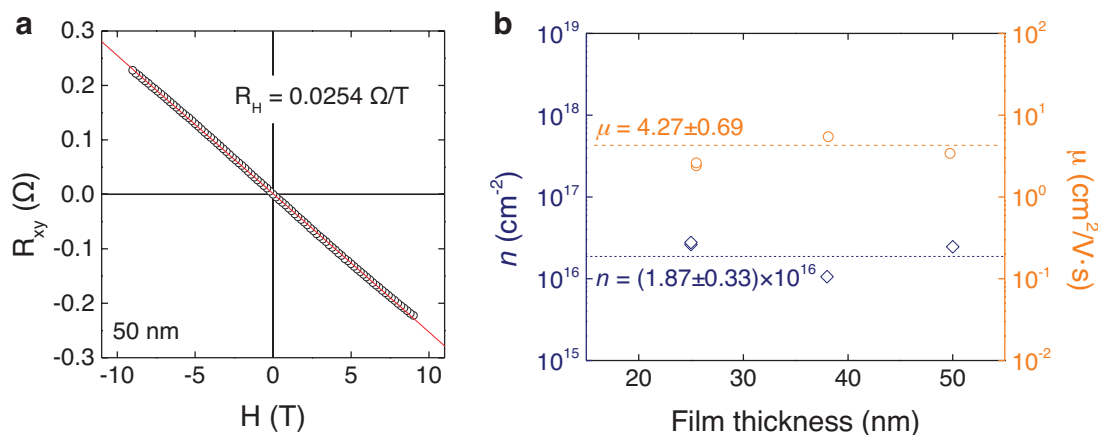


Figure S1. Transport characteristics of SmB_6 thin films. (a) Hall resistivity (R_{xy}) vs. field measured at 2 K for a 50 nm SmB_6 film. (b) Sheet carrier concentration (n) and mobility (μ) for different thickness SmB_6 films.

To further investigate the surface state, we measured the Hall resistance (R_{xy}) as a function of magnetic field, and calculated the carrier concentration and the mobility of the SmB_6 thin films. As shown in Figure S1a, the Hall resistivity R_{xy} of the 50 nm film appears to follow a straight line at 2 K in the entire magnetic field range we studied, suggesting that only one type of carriers contributes the electrical conductivity at 2 K and that bulk contribution is well suppressed: if the bulk contribution persists at such low temperatures, we would expect there to be multiple types of carriers with different concentrations and mobility values, leading to a nonlinear field dependence of R_{xy} as it has been previously observed in other TIs such as Bi_2Se_3 [1,2]. In contrast, the linear field dependence we observed indicates a presence of a single carrier in SmB_6 thin films at 2 K and the insulating bulk state attributed to the Kondo insulating nature.

The slope of $R_{xy}(B)$ is determined by $1/ne$ where n is the sheet carrier concentration. A mobility, μ of carriers can be calculated from $\mu = G_{\square} / en$. We obtain both n and μ for each thin film and plot them as a function of film thickness in Figure S1b. Both n and μ appear to be constant regardless of the variation in the film thickness. The average values of n and μ are $1.87 \times 10^{16} \text{ cm}^{-2}$ and $4.27 \text{ cm}^2/\text{Vs}$, respectively. As expected from the observed behavior of G_{\square} , because the surface conduction is dominant at low temperatures, the transport parameters (n and μ) are also independent of the thickness as seen in Fig. S1b.

- Valence state of the Sm ion near surface

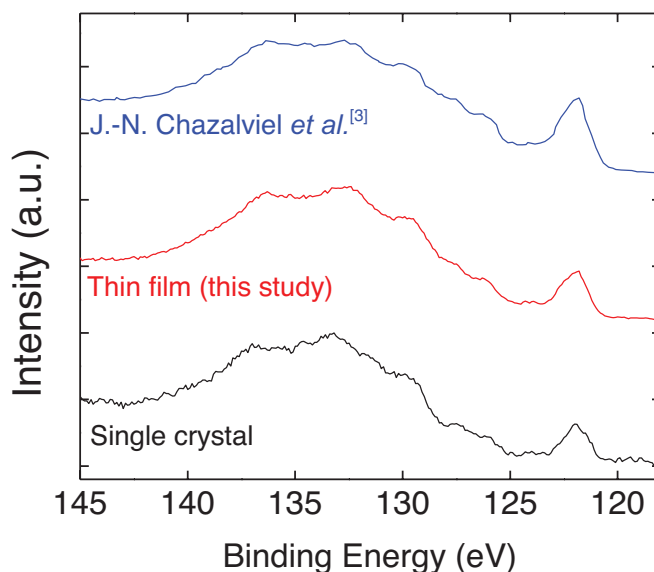


Figure S2. Investigating the valence state of Sm ion in a SmB₆ thin film Comparison of x-ray photoelectron spectroscopy (XPS) Sm 4*d* spectra of a SmB₆ thin film, a single crystal SmB₆ (measured) and bulk[3] (reference)

To investigate the valence state of Sm ions, we used x-ray photoelectron spectroscopy (XPS) to measure the Sm 4*d* spectrum of a SmB₆ thin film. We also measured the Sm 4*d* spectrum of a SmB₆ single crystal as a reference. Details on the single crystal growth and properties can be found elsewhere[4,5]. The Sm 4*d* spectra of the SmB₆ thin film and the single crystal are shown in Fig. S2: the Sm 4*d* spectrum consists of Sm²⁺ and Sm³⁺ related multiplet structures at lower and higher energies than the binding energy of ~ 130 eV, respectively, which partially overlap. As shown in Fig. S2, the Sm 4*d* spectra of the single crystal and the thin film are almost identical, implying that the Sm valence state in the thin film and the single crystal is the same. For comparison, we also included the reported Sm 4*d* spectrum[3] of a bulk SmB₆ sample showing the mixed valence state in the ratio Sm²⁺:Sm³⁺ ≈ 1:3 in Fig. S2. This

looks very similar to both the spectra of the single crystal and the thin film. This indicates that the Sm valence at surfaces of both the thin film and the single crystal is similar to the bulk valence state of SmB_6 (≈ 2.7)[6].

References

1. D. J. Kim, S. Thomas, T. Grant, J. Botimer, Z. Fisk, and Jing Xia, *Surface Hall effect and nonlocal transport in SmB_6 : Evidence for surface conduction*, Sci. Rep. **3**:3150 (2013).
2. N. Bansal, Y. S. Kim, M. Brahlek, E. Edrey, S. Oh, *Thickness-Independent Transport Channels in Topological Insulator Bi_2Se_3 Thin Films*, Phys. Rev. Lett. **109**, 116804 (2012).
3. J. N. Chazalviel, M. Campagna, and G. K. Wertheim, *Study of valence mixing in SmB_6 by x-ray photoelectron spectroscopy*, Phys. Rev. B **14**, 4586 (1976).
4. P. Syers, D. Kim, M. S. Fuhrer, and J. Paglione, *Tuning bulk and surface conduction in the proposed topological Kondo insulator SmB_6* , Phys. Rev. Lett. **114**, 096601 (2015).
5. Y. Nakajima, P. Syers, X. Wang, R. Wang, and J. Paglione, *One-dimensional edge state transport in a topological Kondo insulator*, Nat. Phys. **12**, 213-217 (2015).
6. J. C. Nickerson, R. M. White, K. N. Lee, and R. Bachmann, *Physical properties of SmB_6* , Phys. Rev. B **3**, 2030 (1971).